ELECTRON DENSITY STUDIES IN THE LAVES PHASE $FeBe_2$

M.M.R. COSTA, M.J.M. DE ALMEIDA AND J.A. PAIXÃO

Centro FC1, INIC - Department of Physics - University of Coimbra 3000 COIMBRA, PORTUGAL

[Received January 1992]

ABSTRACT -The main features of the charge density distribution in the hexagonal Laves phase $FeBe_2$ have been deduced from preliminary studies based on X-ray diffraction measurements carried out at room temperature in one single crystal.

Thermal and positional parameters were obtained from a spherical refinement of high order data; final agreement factors R=2.1% and R_w=2.5% were obtained. Difference density maps were calculated using these refined values. Finally the results are summarized and briefly discussed.

1 - INTRODUCTION

The structure of Laves phase compounds with stoichiometric composition AB_2 can be described in terms of the stacking of triangular nets of A and B atoms between Kagamé nets of B atoms. Different possibilities for this stacking give rise to distinct structural types, namely the $MgZn_2$ (C14) and $MgNi_2$ (C36) hexagonal structures and the $MgCu_2$ (C15) cubic structure. These have been first proposed by Friauf [1] and Laves et al. [2]; a review of crystal and band structures and physical properties of Laves phases has been given by Sinha [3].

The size of constituent atoms has been assumed to be determinant in the formation of Laves phase compounds; the ideal ratio R_A/R_B corresponding to closest packing is 1.225. However, several Laves phases are known to exist with values of R_A/R_B ranging from 1.05 to 1.68.

Several authors [4,5] have suggested that a close relationship also exists between the crystallographic structure and the electron concentration e/a. This assumption is supported by the occurrence of phase boundaries for the three types of structure at the same values of e/a, for several systems investigated.

Electron densities in binary Laves phases with transition metals for which $R_A/R_B \neq 1.225$ have been determined in this Laboratory by X-ray diffraction. The deviation of R_A/R_B from the ideal value suggests changes in the valence of the constituent atoms, which should be detectable in careful electron distribution studies.

The presence of two transition elements with rather similar atomic numbers in the Laves phases investigated, $TiCo_2$ [6], $TiMn_2$ [7] and $TiFe_2$ [7] is, in a way, an unfavourable situation when investigating eventual departures from spherical symmetry.

Therefore it was decided to carry out similar studies in the binary Laves phase $FeBe_2$ with only one transition metal, the other constituent being a non transition light element. For this alloy $R_A/R_B = 1.129$.

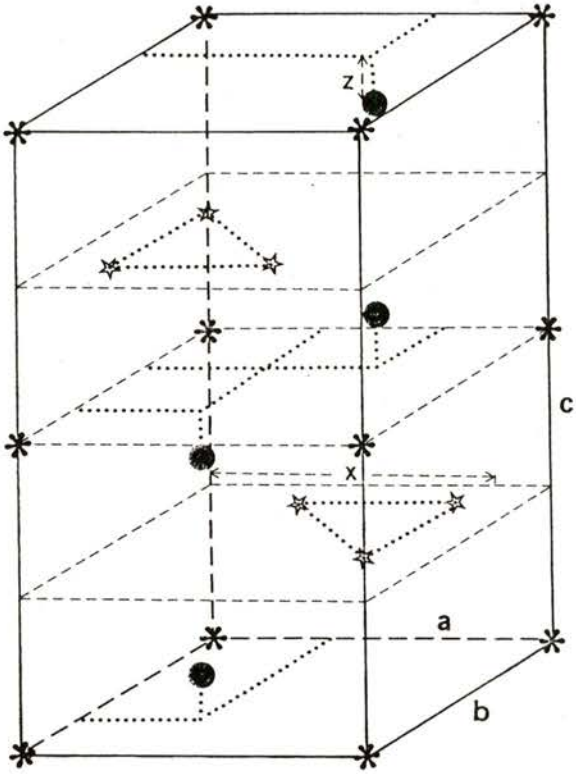

Fig.1 - Unit cell of Laves phase with C14 hexagonal structure: • - Fe atoms; ∗- Be(I) atoms; ☆ - Be(II) atoms

2 - CRYSTAL DATA AND EXPERIMENTAL

The Laves phase $FeBe_2$ has the $MgZn_2$ (C14) hexagonal structure, with space group $P6_3/mmc$. Atomic positions the unit cell are shown in fig.1.

A single crystal with approximate dimensions $(0.07 \times 0.07 \times 0.08)mm^3$ was selected from the material kindly offered by Dr. P.J. Brown, Institut Laüe Langevin, Grenoble, France.

Diffraction data were collected on a single crystal diffractometer CAD4, using Mo-Kα radiation (λ = 0.7017Å) and a graphite (002) monochromator. The absorption coefficient of the alloy for this type of radiation is μ=66.1cm^{-1}.

Lattice parameters were refined using a standard least-squares technique and the CAD4 available software, from 25 reflections with $11.8^\circ < 2\theta < 60.5^\circ$:

$$a = b = 4.2224(10)Å$$
$$c = 6.8700(11)Å$$

$$\alpha = \beta = 90° \; ; \quad \gamma = 120°$$

A set of 6527 independent reflections out to $\sin\theta/\lambda = 1.1 Å^{-1}$ in reciprocal space were measured at room temperature (293±2 K) using ω-2θ scans. For each hkl, up to 24 symmetry-equivalent reflections were measured in order to evaluate and correct for absorption effects.

Five standard reflections were measured every 3 hours; maximum fluctuations of 4% over an exposure period of 272 hours were detected and attributed to variations of the main beam intensity and detector sensitivity. All intensities were rescaled against the standards in order to correct for this effect.

The orientation of the sample was checked after measuring every 60 reflections. Whenever the direction of the scattering vector was found to differ more than 10% from that derived from the UB matrix, a set of 5 reflections previously selected was measured in order to re-orientate the crystal.

3 - DATA ANALYSIS

The analysis of the experimental data was performed with the SDP-Plus programs [8] using a MICROVAX II with VMS operating system.

Lorentz and polarization corrections appropriate to the current geometry were applied to the integrated intensities. An absorption correction based on psi-scans of a few reflections with χ close to 90° and of their geometrically accessible equivalents suggested by North et al [9] was applied to the data. Relevant information concerning this correction is presented in Table 1.

Maximum absorption correction	0.9965
Minimum absorption correction	0.8167
Agreement factors (F_{obs})	0.042

Table 1 - Relevant information concerning absorption correction applied to the data.

Averaging of equivalent reflections was subsequently performed, the total number of non-equivalent intensities being 441. Those average intensities for which $I_{hkl} \leq 3\sigma_{hkl}$, σ_{hkl} being the standard deviation of I_{hkl} , were considered "non-observed"; 129 "observed" reflections were thus obtained.

A set of structure factors for the observed reflections were calculated (F_{calc}) assuming spherical distributions of atomic electrons. Anomalous dispersion corrections were included in the atomic scattering factors using data listed on The International Tables for X-Ray Crystallography [10]. Full matrix least-squares refinements based on $(F_{obs}-F_{calc})^2$ were performed on the observed

data set. A non-Poisson contribution weighting scheme was used, the weight w of each reflection being calculated as

$$w = 1/(\sigma_F)^2$$

with

$$\sigma_F = \sigma_{F^2}/2F$$

and

$$\sigma_{F^2} = [\,\sigma_I^2 + (pF^2)^2]^{1/2}$$

where a value of 0.04 for the instrumental instability factor p was used to downweight the most intense reflections. Positional and anisotropic thermal parameters U_{ij} together with a scale factor S were refined using high angle data which included only 89 reflections with $[(\sin\theta)/\lambda] \geq 0.6\text{Å}^{-1}$ [11]. Refinements were carried out until a shift/e.s.d. ratio smaller than 0.001 was achieved for all the parameters. Using the structure amplitudes of all observed reflections [out to $(\sin\theta)/\lambda = 1.1\text{Å}^{-1}$] and fixing the refined values of the above parameters, an extinction parameter g was independently refined using the approximate relationship:

$$|F_{calc}| = |F_{obs}|\,(1 + gI_{calc})$$

derived by Stout and Jensen [12].
Values of the ratio F_{obs}^{corr}/F_{obs} for reflections with $w(F_{calc}-F_{obs}) \leq 2$, ranged between 1.142 and 1.003. Table 2 shows the results of the above described refinements.

Indep. refl. with I>3σ		129
Indep. refl., I>3σ, sinθ/λ>0.6 Å^{-1}		89
Fe atom		
	z	0.06168(9)
	$U_{11}=U_{22}$	0.00501(7)
	U_{12}	0.00250(4)
	U_{33}	0.00379(7)
Be_1 atom		
	$U_{11}=U_{22}$	0.00141(124)
	U_{12}	0.00070(62)
	U_{33}	0.00815(173)
Be_2 atom		
	x	0.82905(112)
	U_{11}	0.00699(95)
	U_{22}	0.00666(129)
	U_{12}	0.00333(65)
	U_{33}	0.00620(70)
R		2.1%
R_W		2.5%
g		$8.90(52)*10^{-6}$
S		0.76895(230)

Table 2 - Positional, thermal and extinction parameters obtained from least squares refinement.

Anisotropic thermal parameters U_{ij} are based on the following expression for the "temperature factor":

$$T = \exp\,[-2\pi(h^2a*^2U_{11} + k^2b*^2U_{22} + l^2c*^2U_{33} + 2a*b*hkU_{12})]$$

The anisotropy of vibrations of the light atoms Be(I) which are located along the

edges (c-axis) of the unit cell is a striking feature of this structure, and can be inferred either from a comparison of the magnitude of the parameter U_{33} with those of $U_{11}(=U_{22})$ and U_{12}, or from the observation of the ellipsoids of thermal vibrations shown in fig.2 for this atom and (for the sake of comparison) for Be(II).

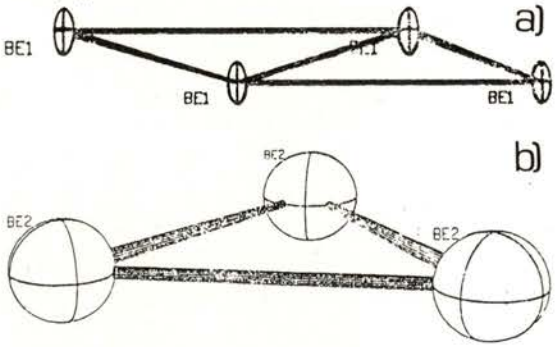

Fig.2 - Ellipsoids of thermal vibrations:
a) Be(I) atoms; axial ratio:5.8
b) Be(II) atoms; axial ratio:0.9

4 - CHARGE DENSITY RESULTS AND CONCLUSIONS.

Fourier analysis of the observed structure factors was performed, the results of which are represented as density maps. The most representative of these, corresponding to sections of the unit cell through different types of atom are shown in fig.3. The electron density around the Fe (fig.3-b) and Be(II) (fig.3-a) atomic positions exhibits no apparent unexpected behaviour.

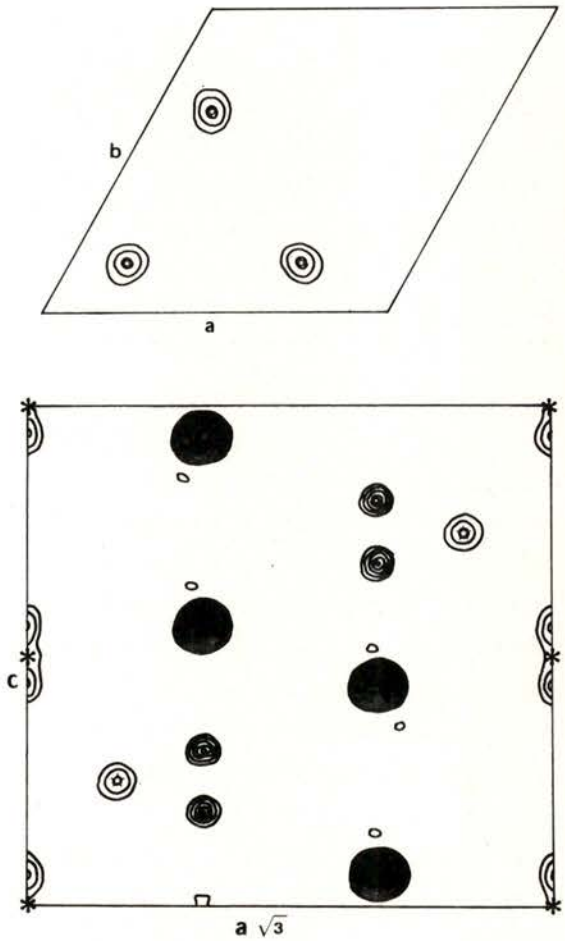

Fig.3 - Fourier maps SF_{obs}. Contour levels at intervals of 10 eÅ^{-3}: • - Fe atoms;* - Be(I) atoms; ☆ - Be(II) atoms.
a)section [00.1] of the unit cell at z=0.25.
b)section [11.0] of the unit cell.

However, at the Be(I) positions (fig.3-b) the density does not have spherical

symmetry; instead two maxima can be seen, symmetrically located with respect to the refined atomic position. Moreover, the density map for section [11.0] (fig.3-b) shows density maxima above and below the triangular arrangement of Be(II) atoms on a line running through the center of the triangles and through the Fe atoms. These maxima correspond to a significantly higher density than that observed at the Be(II) atomic positions.

Subsequent Fourier analysis of the differences (SF_{obs}-F_{calc}) was carried out in order to investigate the origin of the observed effects. The corresponding difference maps are shown in fig.4 the significance level of which can be compared with the error maps in fig.5. The standard deviation of constant regions is 0.3eÅ^{-3}.

Observation of the difference maps shows that both the effect at the Be(I) positions and that occurring below and above the triangles of Be(II) atoms have disappeared.

Hence, it appears that the correction for thermal motion applied to the F_{calc} has taken care of the "anomalies" observed in direct maps. Their origin may therefore be attributed to thermal vibrations perhaps mainly associated with the light Be atoms.

It may also be argued that the models used for correction of absorption and extinction in this crystal are not satisfactory. Furthermore, an eventual twinning effect should also be considered.

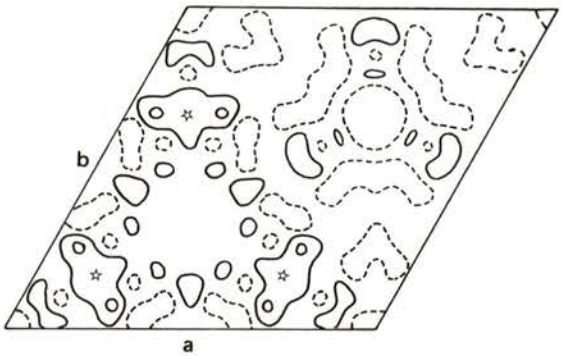

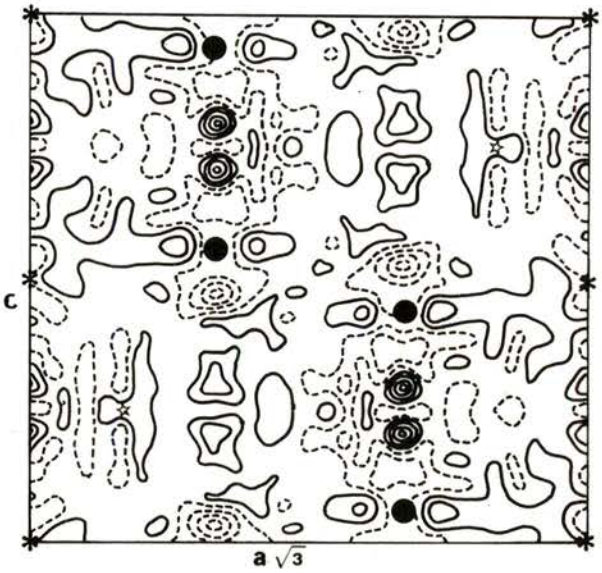

Fig.4 - Fourier difference maps, SF_{obs}-F_{calc}. Contour levels at intervals of 0.4 eÅ^{-3}. First positive contour at 0.2 eÅ^{-3}.

• - Fe atoms; ∗ - Be(I) atoms; ☆ - Be(II) atoms
a)section [00.1] of the unit cell at z=0.25
b)section [11.0] of the unit cell.

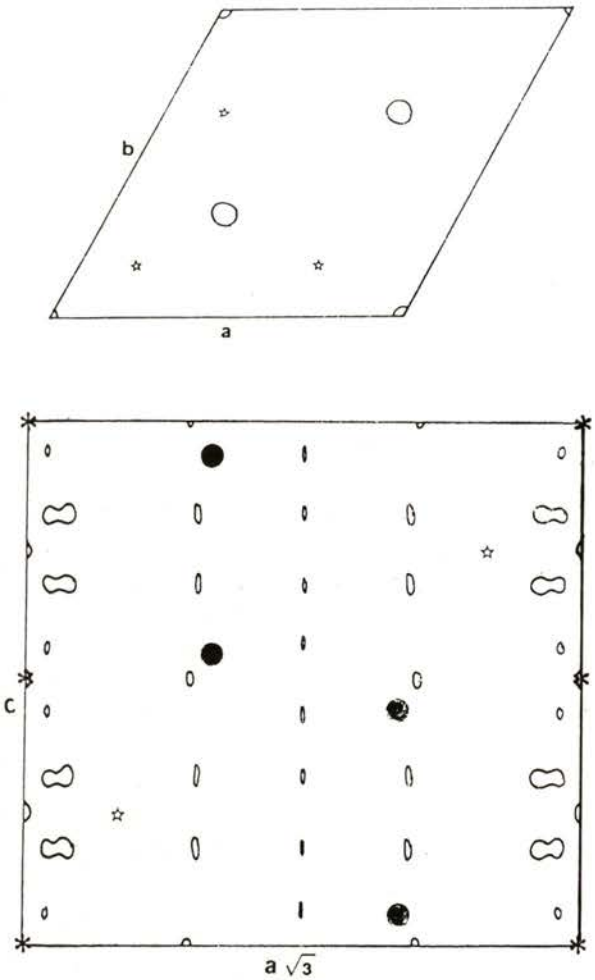

Fig.5 - Fourier maps representing the distribution of errors. Contour levels at intervals of 0.4 eÅ^{-3}. First positive contour at 0.2 eÅ^{-3}.

• - Fe atoms; * - Be(I) atoms; ☆ - Be(II) atoms

a)section [00.1] of the unit cell at z=0.25

b)section [11.0] of the unit cell.

These possibilities will be tested by selecting another crystal with a different shape and volume, for which absorption and extinction effects and eventual twinning should in principle be different.

Significant remaining features on difference density maps are excess density along the direction parallel to the c-axis, both between two nearest neighbour Fe atoms and between two Be(I) atoms. However these effects should not be emphasized until those much stronger, observed on direct maps, are fully explained and their presence in the electron density from a different crystal is confirmed.

ACKNOWLEDGEMENTS

We are indebted to the Cultural Service of the German Federal Republic Embassy, the Deutscher Akademischer Austauschdienst (DAAD) and the German Agency for Technical Cooperation (GTZ) for the offer of a CAD4 automatic diffractometer which enabled the experimental work to be carried out.

REFERENCES

[1] Friauf, J.B., J.Am.Chem.Soc., **49**, 3107 (1927).

[2] Laves, F. and Witte, H., Metallwirtsch. Metallwiss, Metalltech., **14**, 645 (1935).

[3] Sinha, A.K., Progress in Materials Science, **15**, 93 (1972).

[4] Laves, F. and Witte, H., Metallwirtsch. Metallwiss, Metalltech., **15**, 840 (1936).

[5] Lieser, K.H. and Witte, H., Z. Metallkd., **43**, 396 (1952).

[6] Beja, A.M., Alte da Veiga, L., Andrade, L.C.R., Costa, M.M.R. and Paixão, J.A., Portgal. Phys., **19**, 293 (1988).

[7] Almeida, M.J.M, Costa, M.M.R. and Paixão, J.A., Portgal. Phys., **19**, 289 (1988).

[8] Frenz, B.A., Enraf-Nonius Structure Determination Package; SDP Users Guide, Enraf-Nonius, Delft, The Netherlands.

[9] North, A.C.T., Phillips, D.C. and Mathews, F.S., Acta Cryst. **A24**, 351 (1968)

[10] International Tables for X-Ray Crystallography, vol.III, 1974.

[11] Stevens, E.D. and Coppens, P., Acta Cryst. **A31**, 612 (1975).

[12] Stout, G.H. and Jensen, L.H., X-Ray Structure Determination, 410-412, London: Macmillan (1968).